# Control of $P2X_2$ Channel Permeability by the Cytosolic Domain

Angela N. Eickhorst,[2] Amy Berson,[3] Debra Cockayne,[3] Henry A. Lester,[2] and Baljit S. Khakh[1,2]

[1]MRC Laboratory of Molecular Biology, Cambridge CB2 2QH, United Kingdom
[2]Division of Biology, California Institute of Technology, Pasadena, CA 91125
[3]Roche Bioscience, Palo Alto, CA 94304

ABSTRACT ATP-gated P2X channels are the simplest of the three families of transmitter-gated ion channels. Some P2X channels display a time- and activation-dependent change in permeability as they undergo the transition from the relatively $Na^+$-selective $I_1$ state to the $I_2$ state, which is also permeable to organic cations. We report that the previously reported permeability change of rat $P2X_2$ ($rP2X_2$) channels does not occur at mouse $P2X_2$ ($mP2X_2$) channels expressed in oocytes. Domain swaps, species chimeras, and point mutations were employed to determine that two specific amino acid residues in the cytosolic tail domain govern this difference in behavior between the two orthologous channels. The change in pore diameter was characterized using reversal potential measurements and excluded field theory for several organic ions; both $rP2X_2$ and $mP2X_2$ channels have a pore diameter of ~11 Å in the $I_1$ state, but the transition to the $I_2$ state increases the $rP2X_2$ diameter by at least 3 Å. The $I_1$ to $I_2$ transition occurs with a rate constant of ~0.5 $s^{-1}$. The data focus attention on specific residues of $P2X_2$ channel cytoplasmic domains as determinants of permeation in a state-specific manner.

KEY WORDS: ATP • ion channel • modulation • P2X • purinoceptor

## INTRODUCTION

ATP-gated cationic P2X channels define one of the three major families of transmitter-gated ion channels (Khakh, 2001). Although there are seven distinct P2X subunits, much of our understanding is based on studies of the $P2X_2$ subunit which forms homomeric channels. Available evidence indicates that each $P2X_2$ subunit possesses two transmembrane domains, cytosolic $NH_2$ and COOH termini and a large cysteine-rich extracellular loop. There is strong evidence that transmembrane domain 2 (TM2) lines the pore, because mutations here affect organic cation permeability (Khakh et al., 1999; Virginio et al., 1999b) and $Ca^{2+}$ permeability (Migita et al., 2001), and because substituted cysteines in TM2 are modified by extracellular hydrophilic methanethiosulphonate reagents when the channel opens (Rassendren et al., 1997; Egan et al., 1998). The gate appears to be close to a conserved glycine (G342), whereas a conserved aspartate (D349) is internal to it. P2X channel pores are cation selective with almost equal permeability to $Na^+/K^+$ and significant permeability to $Ca^{2+}$.

Some P2X channels also display a time and activation-dependent increase in permeability to organic cations and fluorescent dye molecules before they desensitize. This phenomenon was first reported for, and considered unique to, the $P2X_7$ channel (Surprenant et al., 1996). But subsequent studies demonstrated permeability changes for various recombinant and natively expressed P2X channels in neurons (Khakh et al., 1999; Virginio et al., 1999b). The permeability change of the $P2X_2$ channel is just one example of the recent observations that some channels change their selectivity on the time scale of milliseconds in response to diverse stimuli, including membrane voltage, neurotransmitter binding, and second messengers (Khakh and Lester, 1999). The structural bases and biophysical properties of these changes are poorly understood.

The goal of this study was to provide a more complete understanding of the history-dependent changes in cation permeability at $P2X_2$ channels. We found that the previously reported permeability change of rat $P2X_2$ ($rP2X_2$) channels does not occur at mouse $P2X_2$ ($mP2X_2$) channels expressed in oocytes. We used domain swaps, chimeras, point mutations, reversal potential measurements, kinetics, and excluded field theory to track and quantify permeability changes. Surprisingly, we found that permeation of one $P2X_2$ state ($I_2$) is affected by two specific residues in the cytosolic tail domain, whereas the permeation of a preceding state ($I_1$) is not. We conclude that opening to the $I_2$ state requires conformational changes in the C tail domain, whereas opening to $I_1$ does not.

Address correspondence to Baljit S. Khakh, Division of Neurobiology, MRC Laboratory of Molecular Biology, Hills Road, Cambridge CB2 2QH, UK. Fax (44) 1223-402310; E-mail: bsk@mrc-lmb. cam.ac.uk; or Henry A. Lester, Division of Biology 156-29, California Institute of Technology, 1201 East California Boulevard, Pasadena, CA 91125-2900. Fax: (626) 564-8709; E-mail: lester@caltech.edu

## MATERIALS AND METHODS

### *Cloning, Expression, and Recording*

The $mP2X_2$ cDNA was cloned from a mouse testis library using primers designed to the rat $P2X_2$ cDNA (antisense primer GAA TTC TCA AAG TTG GGC CAA ACC T, sense primer GGA TCC ATG GTC CGG CGC TTG G). Mouse $P2X_2$ cDNA were amplified using PCR Master (Roche) according to manufacturer's instructions. The PCR product was gel purified and cloned into TOPO TA pCR2.1 (Invitrogen) according to manufacturer's instructions. The five individual clones were sequenced (Roche Bioscience sequencing laboratory) on both strands. $mP2X_2$ and $rP2X_2$ cDNA were subcloned into pcDNA3.

The *C tail swap chimeras* were made by digesting $rP2X_2$ and $mP2X_2$ cDNA with HpaI (native site in both cDNAs) and XhoI (in the 3′ polylinker) to produce two fragments: (a) the vector and coding region for the entire $P2X_2$ cDNA, minus part of TM2 and the C tail, and (b) DNA coding for the remainder of TM2 and the COOH-terminal domain. The DNA fragments were separated by agarose gel electrophoresis and purified (QIAGEN gel extraction kit). Thus, the $mP2X_2$ C tail domain was ligated into $rP2X_2$, and vice versa, and restriction analysis was used to confirm the construction.

The *C tail domain chimeras* were constructed in two PCR steps (High Fidelity PCR Master; Roche) using synthetic oligonucleotides (Caltech Polymer Synthesis Facility). In the first step, two PCR reactions produced overlapping pieces, one using $rP2X_2$ as the template and the other using $mP2X_2$ as the template. In the second step, the PCR products from the first steps were used as the template and the final product was a connected chimeric fragment spanning the DNA coding for TM2 through the cytoplasmic tale and into the polylinker. The chimeric fragment and wild-type DNA were digested with HpaI and XhoI. The pieces of the digestion were separated on an agarose gel and extracted. The chimeric fragment and the wild type vector were ligated. Sequencing confirmed the correct chimeras.

Single site mutants were made using Quick Change Mutagenesis (Stratagene). DNA sequencing was used to confirm the mutation. All cDNAs were transcribed in vitro using the mMESSAGE mMACHINE kit (Ambion).

*Xenopus laevis* oocytes were prepared and used for electrophysiological recordings described using described methods. Two-electrode voltage-clamp recording of oocytes was performed using the Geneclamp 500 amplifier (Axon Instruments, Inc.). Electrodes were pulled from borosilicate glass (Sutter Instrument Co.) and back filled with 3 M KCl to yield resistances of 1–2 MΩ. Recordings were made in solution consisting of 98 mM NaCl, 5 mM HEPES, and 1 mM $MgCl_2$ at pH 7.35–7.4, which was superfused over the oocytes by gravity flow at a rate of ~3 ml $min^{-1}$ (chamber volume was ~300 μl). In some experiments, equimolar substitutions of organic cations were made for $Na^+$. The organic cations tested were dimethylammonium, 2-(methyl-amino)-ethanol, $Tris^+$, and N-methyl-d-glucamine. Solutions containing ATP were applied to the oocyte using a solenoid-operated solution switcher (General Valve Company); complete solution exchange around the oocyte occurred within 0.5–1.0 s. Voltage-clamp experiments were controlled by a Digidata 1200 interface and a personal computer running pCLAMP 7 or pCLAMP 8 software (Axon Instruments, Inc.). In some experiments, the voltage was ramped at a rate of 0.36–0.6 mV/ms. Data were filtered at 200–500 Hz and digitized at 3–5 times this rate. Current-voltage relation data were filtered at 1 kHz and digitized at 3 kHz. All experiments were performed at 18–20°C.

### *Data Analysis*

Data were analyzed using Clampfit (Axon Instruments, Inc.) or Origin 5.0 (Microcal Software, Inc.), and appear in the text and graphs as mean ± SEM from *n* determinations as indicated (>4). We employed the principles developed by Hille (Dwyer et al., 1980; Hille, 1992). A transform of the GHK voltage equation under bionic conditions from

$$Erev = \frac{RT}{zF}\ln\frac{P_{X^+}[X^+]_o}{P_{Y^+}[Y^+]_i}$$

to

$$\frac{P_{X^+}}{P_{Y^+}} = ([Y^+]_i/[X^+]_o)\exp(zErevF/RT)$$

provides a way to measure the permeability, P, of ion $X^+$ with reference to ion $Y^+$. However, under the assumption that the intracellular ion concentration is constant, the above equation can be used to measure the permeability of ion $X^+$ relative to $Y^+$, as

$$\frac{P_{X^+}}{P_{Y^+}} = ([X^+]_o/[Y^+]_o)\exp(zF(ErevX^+ - ErevY^+)/RT)$$

where $X^+$ is the organic cation and $Y^+$ is $Na^+$, with a reversal potential close to 0 mV for $P2X_2$ channels (see results). Under fixed ion concentrations this equation simplifies to

$$\frac{P_{X^+}}{P_{Na^+}} = \exp\left(\frac{\Delta ErevF}{RT}\right),$$

where $\Delta E_{rev}$ is the shift in reversal potential and F, R and T have their usual meaning (Khakh et al., 1999). The size of the narrowest region of the pore was determined using excluded field theory (Dwyer et al., 1980; Cohen et al., 1992), which relates ion permeability ratios, and sizes of ions (treated as spheres) to the narrowest region of the pore, which is approximated as a cylinder with a narrow constriction. The theory does not provide information about the shape of the constriction, or the pore, but can be used to measure the dimensions of the narrowest region, as explained below. For a channel pore of radius *Rc*, and ion $X^+$ with a radius *Rx* ($RNa^+$ is the hydrated radius of $Na^+$ at 2.15 Å) the $P_{X^+}/P_{Na^+}$ is given by

$$\frac{P_{X^+}}{P_{Na^+}} = \left(\frac{Rc - Rx}{Rc - RNa^+}\right)^2.$$

A square root transformation gives

$$\sqrt{\frac{P_{X^+}}{P_{Na^+}}} = a - bRx,$$

where

$$a = \frac{Rc}{Rc - RNa^+} \quad \text{and} \quad b = \frac{1}{Rc - RNa^+}$$

and the diameter of the narrowest region of the pore is $2a/b$. In the above equations $a$ and $b$ are obtained from linear regressions of plots of $(P_{X^+}/P_{Na^+})^{1/2}$ versus *Rx* (as in Fig. 4). In such formalisms a convenient check is to determine the diameter of $Na^+$, which is given by $RNa^+ = (a - 1)/b$, and using $a = 1.57$ $Å^{-1}$ and $b = 0.28$ (average from regressions of $rP2X_2$ $I_1$, $mP2X_2$ $I_1$, and $I_2$ shown in Fig. 4). This gives $RNa^+$ as 2.04 Å, which is close to the hydrated radius (Kielland, 1937) of $Na^+$ in water at 2.15 Å. These numbers indicate that there is ~5% error in the calculations reported in this study. The radius of ion $X^+$ (*Rx*) was determined as

TABLE I

*Data for Permeability Changes at rP2X$_2$ Channels for the Experiment Illustrated in Fig. 1*

| | $I_1$ | $I_2$ | $I_{Na^+}$ | *n* |
|---|---|---|---|---|
| Peak current at −60 mV (μA) | 0.5 ± 0.1 | −3.2 ± 1.2 | −10.4 ± 0.5 | 9 |
| Erev (mV) | −66.7 ± 0.9 | −35.1 ± 6.4 | 2.7 ± 0.9 | 9 |
| Slope conductance (μS) | 97 ± 3 | 136 ± 4 | 200 ± 20 | 9 |
| $P_{NMDG^+}/P_{Na^+}$ | 0.07 ± 0.003 | 0.34 ± 0.1 | – | 9 |

The slope conductances, calculated from current-voltage plots over a range of 40 mV around the reversal potential, were significantly different from each other when compared using analysis of variance at $P < 0.05$. For completeness, we also present the individual values for peak amplitudes: $I_1$ 0.2, 0.7, 1.3, 0.5, 0.8, 0.1, 0.6, 0.6, 0.1 μA; $I_2$ –1.9, −1.1, −1.0, −0.5, −4.7, −0.9, −10, −1.3, −7.6 μA; and $I_{Na}$ −10.1, −10.2, −7.4, −9.2, −10.6, −10.5, −12.5, −11.4, −11.6 μA). The $I_{Na^+}/I_2$ ratio was 7.3 ± 1.9 (the ratio for each cell was 5.3, 9.3, 7.4, 18.4, 2.3, 11.7, 1.3, 8.8, 1.5).

$$Rx = \frac{\sqrt[3]{D1 \times D2 \times D3}}{2},$$

where *D*1, *D*2, and *D*3 are the three dimensions of the smallest box that will house the ion. The fold change (Δ) in $P_{X^+}/P_{Na^+}$ is the ratio of $P_{X^+}/P_{Na^+}$ for $I_1$ and $I_2$. Slope conductance values for $I_1$, $I_2$, and $I_{Na^+}$ were measured from current-voltage relationships over a range of 40 mV around the reversal potential. The values were calculated separately for each cell, before averaging. For $I_2$ there was a small difference between these values and those calculated from the average values of I and $E_{rev(NMDG)}$ (as shown in Table I). These differences are expected with small numbers for the numerators, as in the $NMDG^+$ data. For $Na^+$ currents, inward rectification was quantified as $G_{+60\ mV}/G_{-60\ mV}$. Rate constants ($1/\tau$; $s^{-1}$) were determined from single exponential fits to the data. Concentration-effect curves were fitted where appropriate, as indicated, to the Hill equation. Statistical tests were performed using the paired or unpaired Student's *t* test, as appropriate, and a $P < 0.05$ was taken to indicate significance.

## RESULTS

### *Initial Observations with rP2X$_2$ Channels*

Fig. 1 illustrates permeability changes for rP2X$_2$ channels expressed in oocytes, and introduces the measurements that are used throughout this paper. Table I contains data for various measurements from nine cells, from experiments of the type illustrated in the representative waveform shown Fig. 1 A. At a holding potential of −60 mV and in extracellular solutions that contain $NMDG^+$, application of ATP evokes an initial transient outward current (termed $I_1$) at a holding potential of −60 mV. Over a time course of seconds the currents become inward and reach steady-state values ($I_2$), but on switching to $Na^+$ solutions the currents are larger ($I_{Na^+}$; Fig. 1 A). The $I_{Na^+}/I_2$ ratio calculated from the individual cells was 7.3 ± 1.9 ($n$ = 9; Table I legend).

We also measured the reversal potential of the ATP-evoked currents between $I_1$, $I_2$, and $I_{Na^+}$ with voltage ramps (Fig. 1 B), and expressed these values as permeability ratios relative to $Na^+$ (see MATERIALS AND METHODS). The inward $I_2$ current develops with a rate constant ($k_{+1}$ = 0.3 ± 0.01 $s^{-1}$) similar to that for the shift in reversal potential ($k_{+1}$ = 0.4 ± 0.1 $s^{-1}$) from −66.7 mV for $I_1$ to −35.5 mV for $I_2$, thus showing a change in $P_{NMDG^+}/P_{Na^+}$ from 0.07 for $I_1$ to 0.34 for $I_2$ (Table I). The rate constant for the increase in $NMDG^+$ permeability is ∼0.4 $s^{-1}$, similar to that reported previously in mammalian cells (Virginio et al., 1999b). Thus, with time $NMDG^+$ becomes more permeable through rP2X$_2$ pores, but it does not become

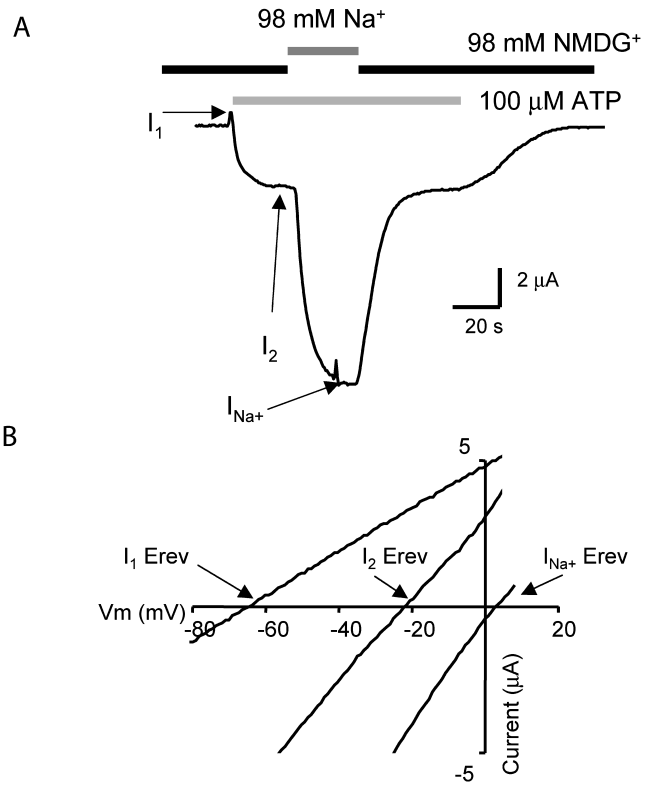


FIGURE 1. Properties of permeability changes at rP2X$_2$ channels. (A) Representative current waveform from a voltage-clamped oocyte (−60 mV). The cell was bathed in an $NMDG^+$-containing extracellular solution and then at the indicated time ATP was applied, first with $NMDG^+$ and then with $Na^+$ in the extracellular solution. The record illustrates the three current phases, $I_1$, $I_2$, and $I_{Na^+}$, the statistics for which are presented in Table I. (B) I-V relations determined at the peak of $I_1$, $I_2$, and at $I_{Na^+}$: note that the reversal potentials differ. The ATP-evoked current reversal potential does not shift over time in extracellular solutions that contain only $Na^+$ (Khakh et al., 1999).

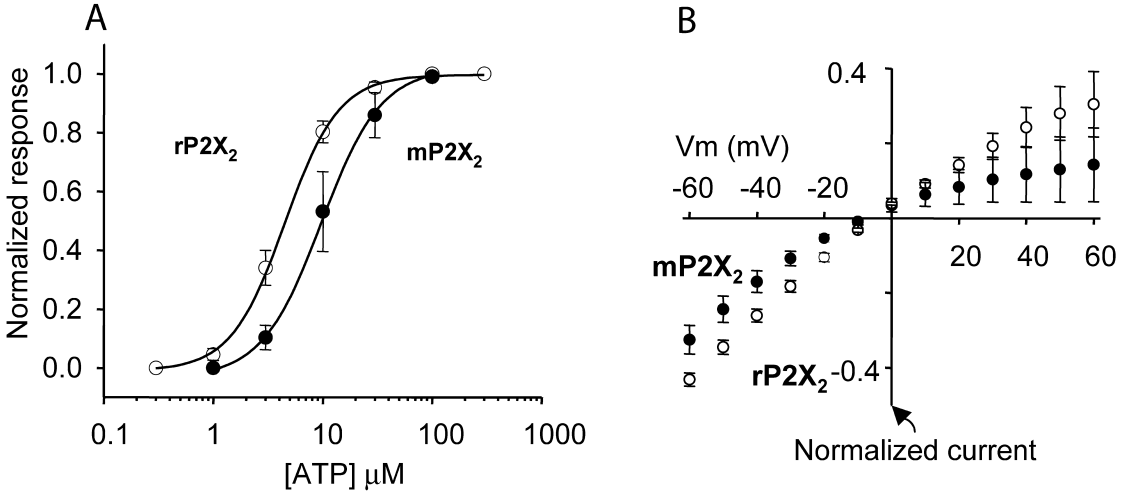


FIGURE 2. Basic properties of $rP2X_2$ and $mP2X_2$ channels. (A) Concentration-effect curves for ATP at $rP2X_2$ and $mP2X_2$. There is a significant difference in $EC_{50}$. (B) I-V relations from voltage steps (−60 to 60 mV in 10-mV steps) for $mP2X_2$ and $rP2X_2$. Note that rectification is approximately equal for both channels, but that there is greater variability in the data for outward currents as compared with inward current. A similar trend for natively and heterologously expressed channels has been reported previously (Khakh et al., 1995; Evans et al., 1996). In this and all other figures the error bars are omitted when they are smaller than the symbols used.

so permeable as $Na^+$ (Erev 2.7 mV; $n = 9$, mean values are shown in Table I).

In the present study $rP2X_2$ channels underwent permeability changes in all batches of oocytes, but the extent of the change varied from batch to batch (for example our results show values for $P_{NMDG+}/P_{Na^+}$ between 0.17 and 0.34). These observations suggest the presence of uncontrolled variable(s) that influence the permeability change. To control for this variability, all comparisons between mutant and wt channels were made from the same batches. The remainder of this paper analyzes the nature of the changes that occur during the growth of the current from $I_1$ to $I_2$, and the accompanying shifts in reversal potentials (Fig. 1, A and B).

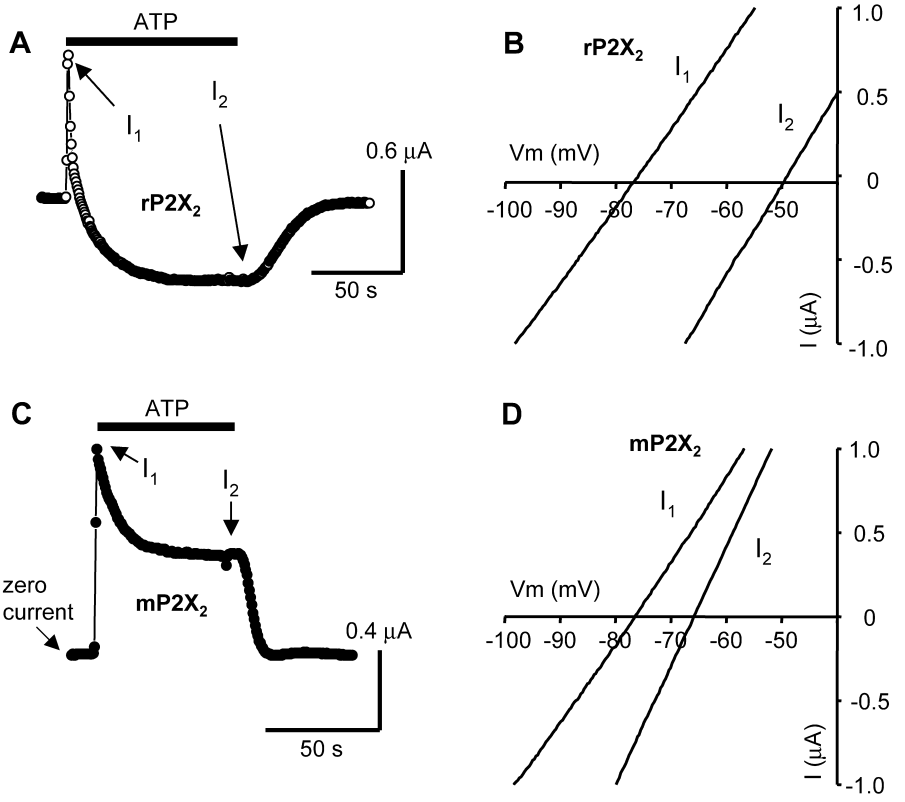


FIGURE 3. $rP2X_2$ and $mP2X_2$ channels differ with respect to permeability changes. (A) $rP2X_2$: steady-state current waveform (−60 mV) in $NMDG^+$ extracellular solutions. ATP was applied when indicated and evoked an outward current that became inward over time. (B) Reversal potentials at the peak of $I_1$ and $I_2$ for $rP2X_2$. (C) $mP2X_2$: steady-state current waveform in $NMDG^+$ extracellular solutions. ATP was applied for the period indicated and evoked an outward current that waned to a steady-state level. (D) Reversal potentials at the peak of $I_1$ and $I_2$ for $mP2X_2$.

*Species Differences Reveal a Rationale to Study the Basis of Permeability Changes*

We cloned and expressed $mP2X_2$ channels in *Xenopus* oocytes. Rat and mouse $P2X_2$ channels were similar with respect to peak $I_{Na^+}$, but the ATP $EC_{50}$s differed, being 2 ± 1 and 12 ± 4 μM with Hill slopes of 1.9 ± 0.2 and 2.0 ± 0.2, respectively, under conditions where we expect the pore to have dilated to the $I_2$ state ($n$ = 5; Fig. 2 A). Because of the difference in $EC_{50}$, and to minimize any errors on the linear part of the curve, all subsequent experiments were performed at saturating concentrations of ATP (≥100 μM). $rP2X_2$ and $mP2X_2$ channels displayed similar current-voltage relations in $Na^+$ solutions: the $I_{Na^+}$ reversal potentials were close to 0 mV (−4.1 ± 0.1 and −6.5 ± 1.5 mV; $P > 0.05$) and the rectification indices ($G_{+60\ mV}/G_{-60\ mV}$) were 0.6 ± 0.2 and 0.5 ± 0.2 ($P > 0.05$), for $rP2X_2$ and $mP2X_2$ (Fig. 2 B). In short, there were no major differences between $rP2X_2$ and $mP2X_2$ channels in $Na^+$ solutions.

When ATP was applied in extracellular solutions that contained $NMDG^+$ in place of $Na^+$ at −60 mV, a clear difference between $rP2X_2$ and $mP2X_2$ channels was apparent. Fig. 3 illustrates this distinction. In $NMDG^+$ solutions application of ATP to $mP2X_2$ evoked an initial outward current ($I_1$), that decreases over 50 s to reach a steady-state value ($I_2$). In contrast, at $rP2X_2$ channels the current actually switches direction: $I_1$ is outward and $I_2$ is inward. Current-voltage relations based on voltage ramps (Fig. 3, B and D) show that the development of $I_2$ for both $rP2X_2$ and $mP2X_2$ channels is associated with shifts in reversal potential over time, but the shift is much greater for $rP2X_2$ than for $mP2X_2$. Thus, for $rP2X_2$ channels $P_{NMDG+}/P_{Na^+}$ is 0.07 ± 0.002 for $I_1$ (500 ± 77 nA), and at the steady-state $I_2$ (−1241 ± 209 nA) the $P_{NMDG+}/P_{Na^+}$ is 0.15 ± 0.007 ($P < 0.01$). In contrast for $mP2X_2$ channels at the initial $I_1$ peak (615 ± 92 nA) the $P_{NMDG+}/P_{Na^+}$ is 0.07 ± 0.003, and at the steady-state $I_2$ current (−12 ± 140 nA) the $P_{NMDG+}/P_{Na^+}$ is 0.09 ± 0.006 ($P < 0.05$). In summary, with time $NMDG^+$ becomes much more permeable through $rP2X_2$ pores, but only slightly more permeable through $mP2X_2$ pores.

*Sizing the $P2X_2$ Pore States Using Excluded Field Theory*

For the above experiments we studied the permeability to $NMDG^+$ (radius ~4.5 Å) because this was the standard protocol in previous work on $rP2X_2$ channels. We next tested the hypothesis that smaller cations also change their permeability during ATP activation of the $rP2X_2$ channel. To address this we used four organic cations (dimethylammonium, 2-(methyl-amino)-ethanol, $Tris^+$ and N-methyl-D-glucamine) with radii between 2.7 and 4.5 Å and determined their permeability relative to $Na^+$ ($P_{X^+}/P_{Na^+}$). While both $mP2X_2$ and $rP2X_2$ channels showed increased permeability in the $I_2$ state to all four test ions, the increases for $rP2X_2$ were much more dramatic. Fig. 4 shows the data plotted on graphs to determine the size of the narrowest part of

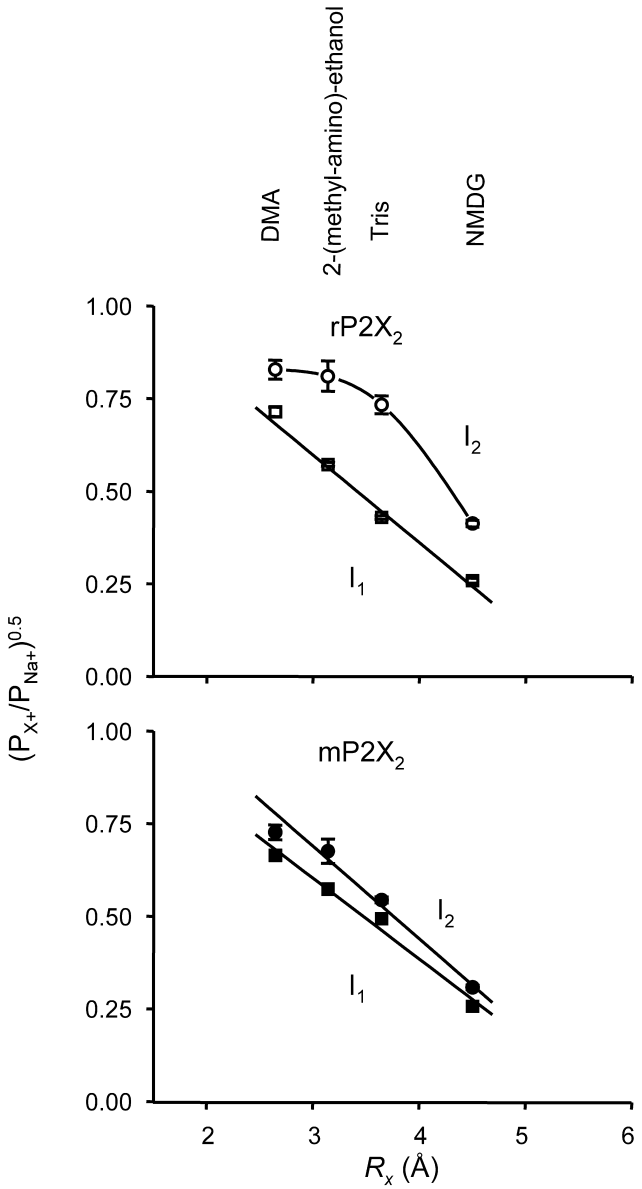


FIGURE 4. Pore sizes determined using EFT. Top and bottom panels show graphs used to determine the narrowest part of the channel pore for $rP2X_2$ and mP2X2 channels, respectively, in $I_1$ (within 1s of applying ATP) and $I_2$ states (up to 30 s after applying ATP). The lines are linear regressions except for $rP2X_2$ $I_2$, which is a cubic spline. Please refer to MATERIALS AND METHODS for details of the pore size calculations. The ions ($R_x$ = radius; see MATERIALS AND METHODS) in order of increasing size are: dimethylammonium (2.7 Å), 2-(methyl-amino)-ethanol (3.1 Å), $Tris^+$ (3.7 Å), and $NMDG^+$ (4.5 Å), and their mobilities in free solution are 51.8, 33.4, 29.4, 24.3, and 50.1 $10^{-4} m^2 S\ mol^{-1}$, for dimethylammonium, 2-(methyl-amino)-ethanol, $Tris^+$, $NMDG^+$, and $Na^+$.

TABLE II

*Experimentally Determined Parameters Used in EFT to Calculate Pore Sizes*

| | *a* ($Å^{-1}$) | *b* | *Rc* = *a*/*b* (Å) | R | *n* |
|---|---|---|---|---|---|
| rP2X2 | | | | | |
| $I_1$ | 1.3 ± 0.002 | 0.23 ± 0.005 | 5.7 | 0.99 | >5 |
| $I_2$ | – | – | – | – | |
| mP2X2 | | | | | |
| $I_1$ | 1.6 ± 0.002 | 0.29 ± 0.01 | 5.5 | 0.99 | >5 |
| $I_2$ | 1.8 ± 0.05 | 0.31 ± 0.01 | 5.8 | 0.99 | >5 |

See MATERIALS AND METHODS for details, but briefly, *Rc* is the radius of the narrowest part of the channel pore, r is the correlation coefficient for the linear regression, and – indicates that a regression was not attempted because the data were clearly nonlinear.

the channel pore, using excluded field theory (EFT).* EFT was used previously to size the muscle nicotinic channel pore at a diameter of 6.5–8.4 Å (Dwyer et al., 1980; Cohen et al., 1992), which agrees well with the pore diameter revealed by imaging the open channel (Unwin, 1995). Using EFT we determined the diameter of the narrowest part of the $rP2X_2$ pore in the $I_1$ state as 11.4 Å, which is similar to the $mP2X_2$ pore $I_1$ states at 11.0 Å, and 11.6 Å diameter in the $I_2$ states (Table II).

Thus, both $I_1$ and $I_2$ states of the $mP2X_2$ channel, as well as the $I_1$ state of the $rP2X_2$ channel, have diameters equal to within 10%, but markedly smaller than the $rP2X_2$ $I_2$ state (Fig. 4); what is the size of the latter state? The data at hand do not give an accurate estimate because all tested organic cations acquired significant permeability. For example, the permeabilities (relative to $Na^+$) of $Tris^+$ and 2-(methyl-amino)-$ethanol^+$ were 0.5 and 0.7, are roughly proportional to their mobilities in free solution (0.6 and 0.7 for $Tris^+$ and 2-(methyl-amino)-$ethanol^+$, relative to $Na^+$) for the $rP2X_2$ $I_2$ state, whereas for the $I_1$ state the permeability values decline more steeply than mobility with $R_x$, as expected for ions that are slowed by interactions with the channel wall as they traverse the $I_1$ state pore (the free solution mobility values are presented in the legend for Fig. 4). On the basis of the plots shown in Fig. 4 we can state that the $rP2X_2$ $I_2$ state diameter is at least 3 Å larger than the ~11 Å that characterizes the $rP2X_2$ $I_1$ and $mP2X_2$ $I_1$ and $I_2$ states. This change increases the area across the narrowest region in the $rP2X_2$ pore by at least ~60 $Å^2$, for a circular filter, or ~76 $Å^2$ for a square filter.

### *A Role for the C Tail in Permeability Changes*

What is the structural basis for the differences between $rP2X_2$ and $mP2X_2$ with respect to $I_2$? As expected, the mouse cDNA has all the hallmarks of a bona fide P2X channel (North, 1996; Khakh, 2001), including sequence identity in TM2 with $rP2X_2$. An alignment for

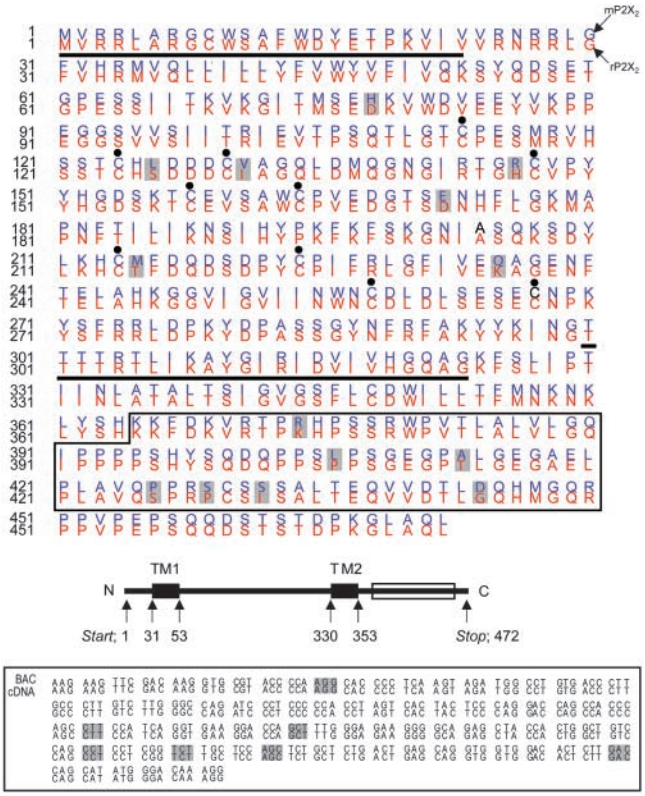


FIGURE 5. Comparison of $rP2X_2$ and $mP2X_2$ sequences. The top panel shows an alignment for the entire $rP2X_2$ and $mP2X_2$ protein sequences (black lines are above predicted transmembrane domains and the black dots indicate the conserved cysteine residues), whereas the middle panel shows a representation of P2X subunit topology. The bottom panel shows an alignment of the $mP2X_2$ cDNA used in this study, and the corresponding sequence of the $mP2X_2$ gene. The codons for the amino acids that differ between $mP2X_2$ and $rP2X_2$ are shown in gray. Note that the genomic sequence agrees with the cDNA sequence in each case, assuring that the $mP2X_2$ cDNA contains no PCR errors. The boxed regions correspond to identical sequence.

the $rP2X_2$ and $mP2X_2$ protein sequence is shown in Fig. 5. Of 472 residues, 14 differ between $rP2X_2$ and $mP2X_2$, but none are in the pore segment (Rassendren et al., 1997; Egan et al., 1998), near the presumed ATP binding sites (Ennion et al., 2000; Jiang et al., 2000) or in TM1 a region known to influence the link between ATP binding to gating of the pore (Haines et al., 2001; Jiang et al., 2001). Seven residue differences between $rP2X_2$ and $mP2X_2$ map to the extracellular loop and the other seven are in the 119-residue COOH-terminal cytosolic domain (Fig. 5). Although intact C tail domains are not critical for P2X function, $rP2X_2$ splice variants that have shorter C tail domains display faster desensitization (Simon et al., 1997; Koshimizu et al., 1998, 1999; Smith et al., 1999), and truncation of C tail domains impairs permeability in some P2X channels (Virginio et al., 1999b). We reasoned that a comparative study between $rP2X_2$ and $mP2X_2$ channels would

*Abbreviation used in this paper: EFT, excluded field theory.

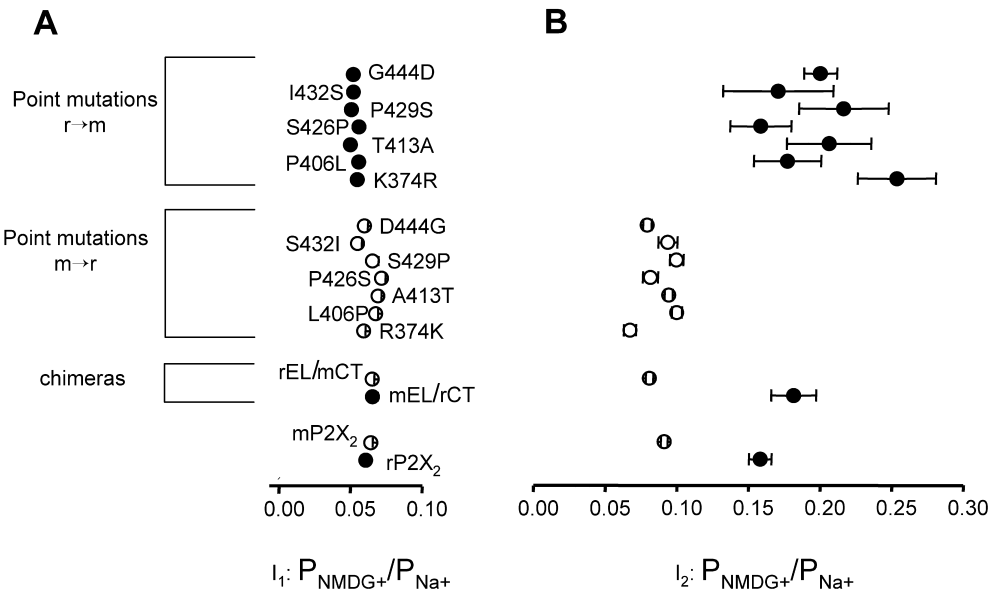


FIGURE 6. No single amino acid residue in the COOH-terminal domain accounts for the differences between $mP2X_2$ and $rP2X_2$ channels. The scatter graphs show data for wt $mP2X_2$, $rP2X_2$, mEL/rCT, rEL/mCT, and 14 single point mutant channels: (A) $I_1$ $P_{NMDG+}/P_{Na+}$ and (B) $I_2$ $P_{NMDG+}/P_{Na+}$. ATP-evoked currents for all mutants, chimeric, and wild-type channels were similar in amplitude for recordings in $Na^+$ solutions, indicating approximately equivalent membrane expression.

represent a direct way to identify residues in the C tail domain that affect permeation.

*Focusing on Residues that Are Permissive for Permeability Changes in the C Tail Domain*

Fig. 5 highlights the differences in the C tail domains between $rP2X_2$ and $mP2X_2$. In our initial experiments, we asked which of the 14 amino acid differences between $rP2X_2$ and $mP2X_2$ determine the presence of $I_2$ and the associated increases in $P_{NMDG+}/P_{Na+}$ in $rP2X_2$, but not in $mP2X_2$? Moreover, can $rP2X_2$ $I_2$-like phenotypes be imparted on to $mP2X_2$ channels by swapping an appropriate domain? To this end we made chimeric channels. For example, transplanting the entire $rP2X_2$ C tail domain onto $mP2X_2$ (mEL/rCT) produced functional responses that were indistinguishable from those of $rP2X_2$ with respect to $I_1$ $P_{NMDG+}/P_{Na+}$ and $I_2$ $P_{NMDG+}/P_{Na+}$ (Fig. 6). Conversely, transplanting the $mP2X_2$ C tail domain onto $rP2X_2$ (rEL/mCT) gave rise to responses that were identical to those of $mP2X_2$ channels. Seemingly, the differences between $rP2X_2$ and $mP2X_2$ reside entirely in the seven residue differences in the C tail domain, illustrated in Fig. 5. But which residues are involved?

We next asked whether any single amino acid is sufficient to make $mP2X_2$ resemble $rP2X_2$, and vice versa. Analysis of the seven appropriate single-site mutants in $mP2X_2$ and the complementary seven mutants in $rP2X_2$ indicate that this is not the case (Fig. 6): for simplicity these mutants have been pooled in Figs. 7 and 8. Thus, any one $rP2X_2$ residue is not enough to endow the $mP2X_2$ with $I_2$, and any one $mP2X_2$ residue is not enough to impair $I_2$ in $rP2X_2$ (Fig. 6). Between two and seven residues are needed to switch the $I_2$ phenotype between $mP2X_2$ and $rP2X_2$.

We next made a series of chimeras in the C tail domain with progressively increasing numbers of $rP2X_2$ C tail domain residues in the $mP2X_2$ C tail domain. This approach tests for effects of substituting sequential residues, beginning at the end of the tail. Results are shown in Fig. 7. Remarkably, from the data it is clear that the last (most COOH-terminal) two amino acids, of the seven differences between $mP2X_2$ and $rP2X_2$, are sufficient to confer $rP2X_2$-like behavior on the $mP2X_2$ channel with respect to the $I_2$ and $P_{NMDG+}/P_{Na+}$ changes. We call this chimera m430r, because until residue 430 the sequence is $mP2X_2$, and after residue 430 the sequence is $rP2X_2$. Increasing the number of $rP2X_2$ residues from two to four produces progressively smaller increases in the $I_2$ phenotype, but clearly the largest jump occurs for transplantation of the last two residues. In $rP2X_2$ they are I432 and G444 and for $mP2X_2$ these residues are S432 and D444 (Fig. 5).

We also made the reverse series of chimeras, with progressively increasing numbers of $mP2X_2$ C tail domain residues in the $rP2X_2$ C tail domain. Here again a clear picture is apparent: the last two $mP2X_2$ residues are sufficient to eliminate $I_2$ and $P_{NMDG+}/P_{Na+}$ changes. Increasing the number of $mP2X_2$ residues in the $rP2X_2$ tail from two to four produces no greater effect than simply substituting two (Fig. 7).

There are two outliers to the trend (shown by gray arrows). Transplantation of five $rP2X_2$ residues into $mP2X_2$ (m407r) produces a channel that desensitizes rapidly within 1–2 s, whereas the other mutants resemble wt $rP2X_2$ and desensitize negligibly over a time period of up to 60s. Similarly, transplanting four $mP2X_2$ residues into rP2X2 produces a channel that expresses poorly and desensitizes completely. In this chi-

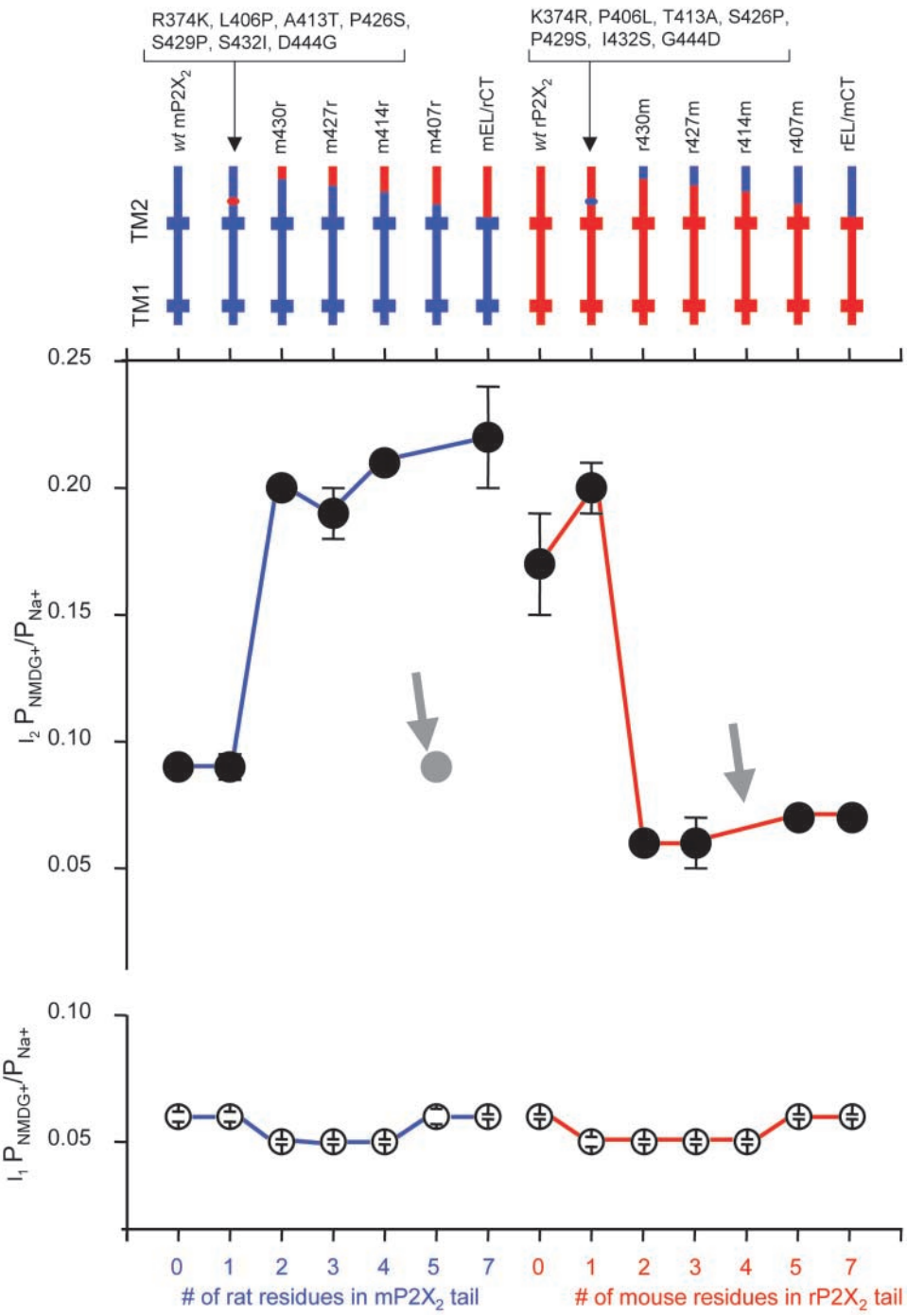


FIGURE 7. Identification of C tail domain residues that govern permeability changes in the $P2X_2$ channel. The top panel illustrates the location of $P2X_2$ channel mutants, and chimeras with respect to the two TM domains. The bottom panel shows $P_{NMDG+}/P_{Na+}$ for the $I_2$ and $I_1$ states. Note that $I_1$ $P_{NMDG+}/P_{Na+}$ is constant for all channels, but $I_2$ $P_{NMDG+}/P_{Na+}$ varies depending on the composition of the C tail domain. Thus $rP2X_2$ channels undergo large changes between $I_1$ and $I_2$, whereas $mP2X_2$ channels do not. The differences can be reversed by transplanting the C tail domains (mEL/rCT and rEL/mCT) and by making chimeras that include the two most COOH-terminal $rP2X_2$ residues of the seven that differ in this domain (see Fig. 5). The gray arrows point to uninformative or outlier constructs.

mera, reversal potentials could not be measured at a time point when $I_2$ is expected to occur; therefore, these constructs are not informative with respect to changes in permeability. For these chimeras we expect that the channels close before spending appreciable time in the $I_2$ state. This behavior is similar to our previous data with $rP2X_1$ and $rP2X_3$, which also desensitize rapidly, and previous work with $P2X_2$ channels that indicate mutants in the C tail domain affect desensitization (Smith et al., 1999).

### *Permeability Changes Are Unrelated to $I_1$, but Correlate with the Growth of $I_2$*

The dataset presented in this study allows us to address a number of questions about the relationships between $I_1$ and $I_2$ states. For instance, is the extent of pore dilation in the $I_2$ states determined by the permeability of the preceding $I_1$ state? In other words, do channels with a lower $P_{NMDG+}/P_{Na+}$ in the $I_1$ state result in a lower $P_{NMDG+}/P_{Na+}$ for the $I_2$ state, and vice versa?

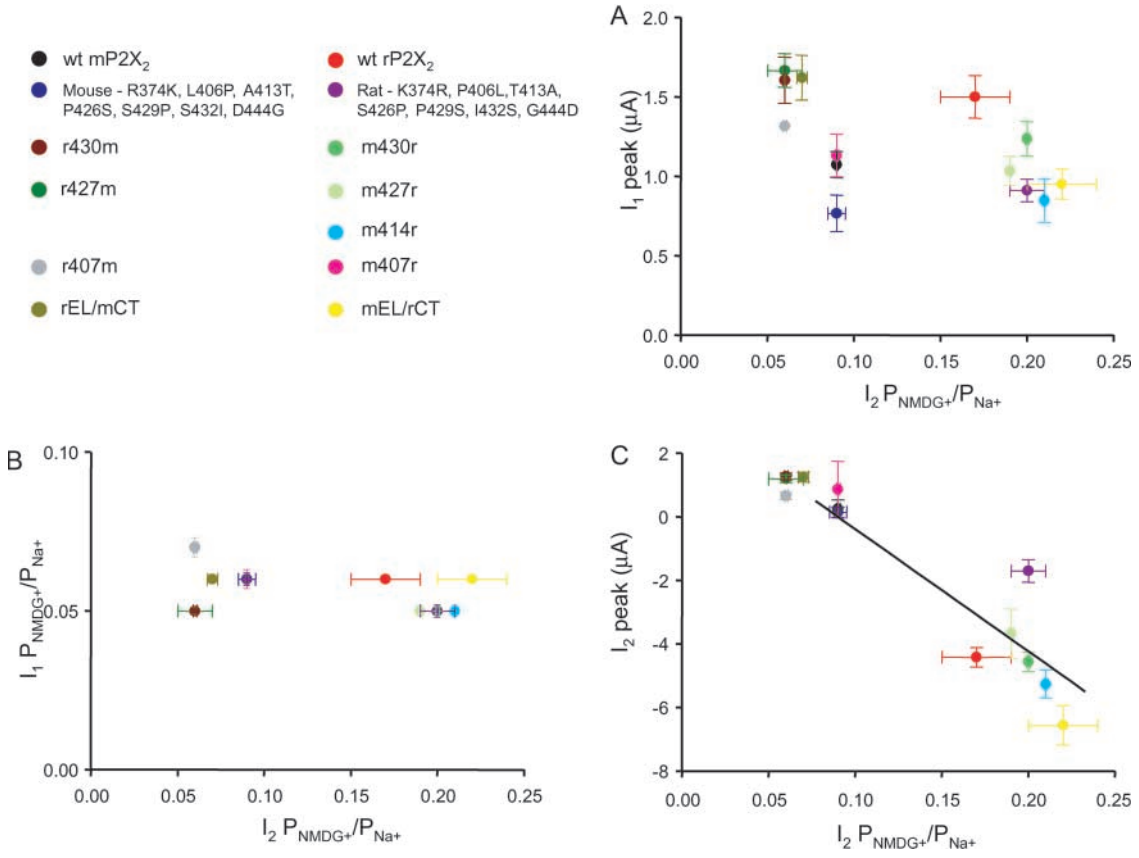


FIGURE 8. Relationship of permeability changes to steady-state currents, $I_1$ and $I_2$. (A) The relationship between $I_1$ amplitude and $I_2$ $P_{NMDG+}/P_{Na+}$. (B) The relationship between $I_1$ $P_{NMDG+}/P_{Na+}$ and $I_2$ $P_{NMDG+}/P_{Na+}$. (C) The relationship between $I_2$ amplitude and $I_2$ $P_{NMDG+}/P_{Na+}$; the two parameters are well correlated ($r = 0.9$). We verified that slope conductance values followed a similar trend to current peak amplitudes for the majority of mutants where such data was available. For this figure, the single point mutants shown in Fig. 6 have been pooled, and there is no point for the r414m chimers because there was no measurable $I_2$.

Moreover, are $P_{NMDG+}/P_{Na+}$ changes related to $I_1$ amplitude, and therefore ion flow? There was a clear correlation for all point mutants, chimeras, tail swaps, and *wt* channels between $I_2$ amplitude and $I_2$ $P_{NMDG+}/P_{Na+}$ changes, but not between $I_1$ amplitude and $I_2$ $P_{NMDG+}/P_{Na+}$ (Fig. 8), arguing that the extent of pore dilation in the $I_2$ state is not related to ion flow in the $I_1$ state. There was also no correlation between $I_1$ $P_{NMDG+}/P_{Na+}$ and $I_2$ $P_{NMDG+}/P_{Na+}$. We next asked, do permeability changes merely happen secondarily to the growth of $I_2$ or do they mirror it? Table III shows the rates for increases in $P_{NMDG+}/P_{Na+}$, as well as for the growth from $I_1$ to $I_2$ for $rP2X_2$, mEL/rCT, and m430r channels. The rate constants for $rP2X_2$, mEL/rCT, and m430r channels are the same for $P_{NMDG+}/P_{Na+}$ changes and growth of $I_2$ from $I_1$ at −60 mV. Overall, these data show that (a) $I_2$ amplitude and $P_{NMDG+}/P_{Na+}$ provide measures of the same underlying phenomenon because they are well correlated and occur with the same rates across a range of mutants, and (b) $P_{NMDG+}/P_{Na+}$ changes are not a consequence of ion flow during the outward $I_1$. Moreover, the data clearly show that whereas the tail swaps and chimeras produce profound effects on $I_2$, they have no effect on $I_1$ amplitude or $I_1$ $P_{NMDG+}/P_{Na+}$ across experiments from 26 distinct channels (2 wild type channels, 14 point mutations, 10 chimeras; Figs. 6–8). A lack of effect on $I_1$ serves as an internal control

TABLE III

*Rate Constants for Development of $I_2$ and Increase in $P_{NMDG+}/P_{Na+}$ for wt and Engineered $P2X_2$ Channels*

| | Rate | | |
|---|---|---|---|
| | Growth $I_1$ to $I_2$ | Increase in $P_{NMDG+}/P_{Na+}$ | *n* |
| | $s^{-1}$ | $s^{-1}$ | |
| *wt* rP2X2 | 0.5 ± 0.09 | 0.5 ± 0.07 | 6 |
| mEL/rCT | 0.4 ± 0.03 | 0.3 ± 0.02 | 6 |
| m430r | 0.4 ± 0.06 | 0.4 ± 0.09 | 6 |

Rate constants ($1/\tau$) were determined from single exponential fits to the growth of steady state current from $I_1$ to $I_2$ as illustrated in the waveform of Fig. 1 A, and for the increase in $P_{NMDG+}/P_{Na+}$ over time they were determined from current-voltage relations like those illustrated in Figs. 1 B and 3.

against any effects on overall protein conformation. But more so the data sharply focus attention on amino acids that specifically affect permeation of a channel state: $I_2$.

## DISCUSSION

There is convincing evidence that the $P2X_2$ channel COOH-terminal domain is cytosolic, including studies of functional concatenated subunits and access of antibodies raised to the cytosolic domain in permeabilized, but not non permeabilized cells (Torres et al., 1998; Stoop et al., 1999). The main finding of the present study is a significant extension and sharpening of the view that the COOH-terminal cytosolic domain affects permeation of the P2X channels in a dilated state. We exploited the observation that rat $P2X_2$ ($rP2X_2$) channels display a much more robust history-dependent permeability change than do mouse $P2X_2$ ($mP2X_2$) channels. The present study shows that replacement of just two amino acid residues abolishes the change in permeability in $rP2X_2$, and just two residues allows $mP2X_2$ channels to undergo permeability changes. The "negative controls" of the $mP2X_2$ channel and of the various $rP2X_2/mP2X_2$ chimeras, which show identical physiology in the $I_1$ state but completely different physiology in the $I_2$ state, allow us to conclude even more confidently that the $I_2$ state is not an artifact of voltage-clamp fidelity, $Ca^{2+}$-activated conductances, or any other vaguely imaginable event. Instead, the $I_2$ state results from a change in the pore, in a transition that is discussed below.

Our finding that the pore dilates by at least 3 Å is consistent with measurements using dye uptake studies (Khakh et al., 1999; Virginio et al., 1999a,b). Because cationic dye flux studies are interpreted in a binary fashion (the dye either permeates or not), they provide a cutoff for the pore size. For instance, YOPRO1 (16.8 × 12.8 × 8.2 Å) does not permeate P2X channels that lack the $I_2$ state because two of its dimensions are larger than the $I_1$ pore, which we estimated to be 11 Å in the present study for $P2X_2$ channels. However, YOPRO1 permeability through $P2X_2$ channels increases in a time-dependent manner during ATP application, reaching steady-state in 30–50 s. This time course is slower than opening to the $I_1$ state, which occurs in <300 ms (Fig. 1 A), but resembles the time for opening to the dilated state (Fig. 1 A), as measured either by the growth of $I_1$ to $I_2$, or by increases in $P_{NMDG+}/P_{Na+}$. These data imply that YOPRO1 does not permeate the 11 Å $I_1$ states because of steric hindrance, but can permeate the dilated $I_2$ state. These considerations imply that the pore of P2X channels must dilate by at least 2 Å, consistent with the electrophysiological data presented in this study indicating that the pore dilates by at least 3 Å. A more accurate estimate of $I_2$ pore size is required, but the present paucity of approximately spherical monovalent cations larger than $NMDG^+$ vitiates further EFT experiments. Moreover, an attempt to use polymers of variable length has proved unfruitful (Virginio et al., 1999a). Perhaps novel approaches are required to accurately size the $I_2$ state.

We compare our data to observations on $P2X_7$ channels. Early studies of $P2X_7$ channels carrying a truncated C tail suggested a role for the C tail domain in permeability changes, but did not pinpoint individual or stretches of important residues (Surprenant et al., 1996). A single nucleotide polymorphism of the $P2X_7$ channel gene in a population of humans with deficits in lymphocyte and monocyte function results in functionally impaired, but appropriately membrane localized, $P2X_7$ channels carrying a E496A mutation in the COOH-terminal tail domain (Gu et al., 2001). These observations support our present findings that distinct COOH-terminal domain residues affect P2X channel function, but our data are enlightening because they suggest a molecular explanation for the functional deficits in humans with the $P2X_7$ channel E469A polymorphism (Gu et al., 2001). In the simplest case, polymorphic E469A channels display impaired dye uptake through the $I_2$ states (Gu et al., 2001) because the C tail domains are locked in a nonpermissive state, as revealed by the appropriate mutants and chimeras reported here. The two nonpermissive residues identified in this study (S432 and D444 in $mP2X_2$) and the E469A mutation in human polymorphic $P2X_7$ channels all locate to a region of the C tail domain that is ~100 residues from the pore-lining segment.

### *Permeability Measurements and Conductances*

The present study adds quantitative details on the extent of the change from a relatively selective $I_1$ state to a less selective $I_2$ state, which permeates organic cations with ease. Our most complete dataset, for $NMDG^+$, allows us to compare three related parameters for $NMDG^+$ permeation in the $rP2X_2$ $I_2$ state: relative free solution mobility, relative conductance, and relative permeability. For the experiment specifically designed to compare permeability and conductance, these parameters for $NMDG^+$ are, respectively, 0.49 (Barry and Lynch, 1991; Ng and Barry, 1995), 0.68 (Table I), and 0.34 (Table I), relative to $Na^+$. As noted in RESULTS, the absolute magnitude of the permeability change varied somewhat between batches of oocytes, and the measured $P_{NMDG+}/P_{Na+}$ range was 0.17–0.34 across all our experiments. The slope conductance for $NMDG^+$ in the $I_2$ state is therefore surprisingly high relative to that for $Na^+$.

Conductance is governed by several mechanisms not directly related to permeability, which primarily reflects a single rate-limiting filter. The interestingly high ratio

of macroscopic $NMDG^+$ to $Na^+$ conductance calls for single-channel measurements of the $I_2$ state. The pioneering single-channel studies of $P2X_2$ channels (Ding and Sachs, 1999a,b) have not systematically explored the optimal conditions for production of the $I_2$ state (Khakh et al., 1999; Virginio et al., 1999b): very low extracellular $Ca^{2+}$ and concentrations of ATP >10 μM (Virginio et al., 1999b). Moreover, $rP2X_2$ channels in excised patches display inactivation kinetics that are quite different to those in whole-cell mode, implying the loss of necessary cytosolic components (Ding and Sachs, 2000).

In the absence of single-channel $I_2$ state recordings, we review several previously reported single-channel characteristics of the $I_1$ state in monovalent metal cation solutions ($NMDG^+$ single-channel currents are below the resolution of this state). At least two mechanisms decrease the macroscopic conductance (Ding and Sachs, 1999b). There is an $Na^+$ ion binding site ~20% of the distance through the electric field (from the outside), with an affinity of ~90 mM at −60 mV (Ding and Sachs, 1999a). Under our conditions, this site would be 50% saturated. Single-channel recordings also show pronounced flickering; the maximal open probability is 0.6. One of these mechanisms might operate more strongly for $Na^+$ than for $NMDG^+$ in the $I_2$ state, accounting for the interestingly high ratio of $NMDG^+$ to $Na^+$ slope conductance.

*Toward a View of P2X Channel Gating*

We observed profound effects for point mutants, chimeras, and tail swaps on $I_2$ amplitude and $I_2$ $P_{NMDG+}/P_{Na+}$ changes, but no effect on $I_1$ amplitude or $I_1$ $P_{NMDG+}/P_{Na+}$. A lack of effect on $I_1$ across experiments from 26 distinct channels serves as a good internal control against effects on overall protein conformation, and strongly argues that the effect of the mutants and chimeras is specific to the permeation of the $I_2$ state. With this control dataset in hand we can conclude that residues in the C tail affect the $I_2$ state. But what are the structural details of this transition? P2X channels are the newest members of the transmitter-gated ion channels to be identified, they have little sequence homology with any other ion channels and relatively little is known about their structure-function relationships. Nonetheless, we present some plausible views.

Present evidence indicates that ATP binds to regions just extracellular to the transmembrane domains in P2X channels (Ennion et al., 2000; Jiang et al., 2000). In the present view, ATP binding causes motions in TM1 (Haines et al., 2001; Jiang et al., 2001), perhaps as the outer part of TM1 moves with respect to the outer part of TM2, that allow the pore to open at or near G342 in TM2 (Rassendren et al., 1997; Egan et al., 1998; Migita et al., 2001). Our data suggest (Fig. 9) that

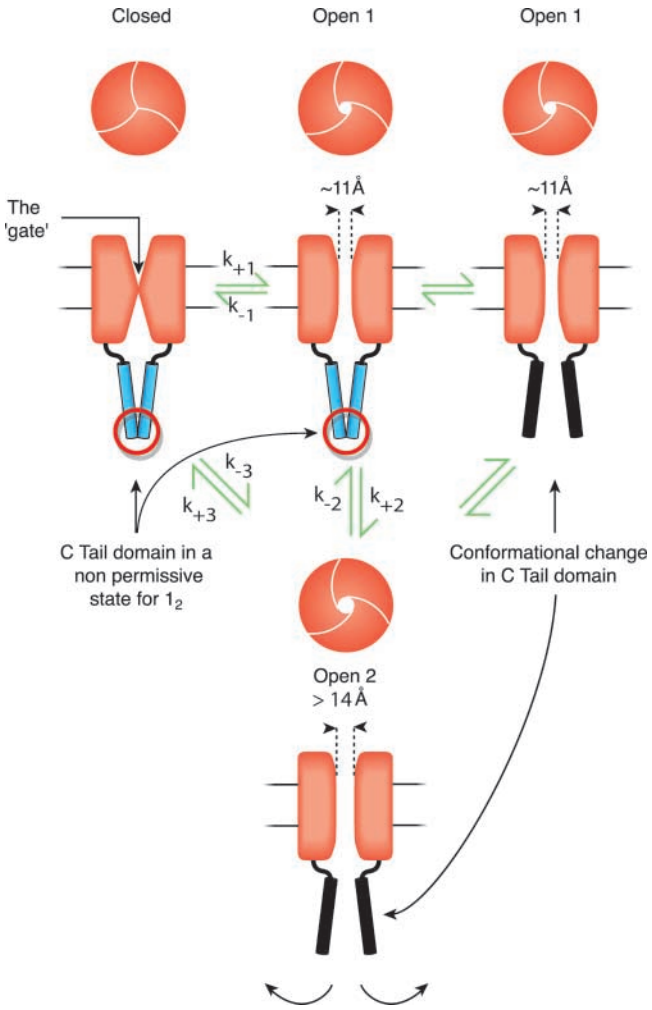


FIGURE 9. A summary of $rP2X_2$ permeability changes. The cartoon shows $rP2X_2$ channels in closed and open states of differing diameter across the narrowest region. The narrowest region is shown as the gate. In the Closed and Open 1 state the C tail domain is diagrammatically shown as in a "nonpermissive state" with respect to permeability changes. The present paper shows that a conformational change occurs in the tail as, or before, the pore dilates, and this is hypothetically shown as a motion of the C tail domain away from the inner aspect of the channel, as in MscL channel gating (Sukharev et al., 2001). The model implies the existence of a state where the tail has undergone a conformation change but the pore has not yet dilated. A direct transition from Closed to Open 2 was demonstrated previously for mutant channels (Khakh et al., 1999; Virginio et al., 1999b).

the transition from $I_1$ to $I_2$ increases the area across the narrowest region in the $rP2X_2$ pore by at least ~60 $Å^2$, for a circular filter, or ~76 $Å^2$ for a square filter. This implies an increase in the pore diameter by at least 3 Å, but an accurate estimate of the $I_2$ state pore size requires further work. The change is regulated by the disposition of side chains in a particular region of the cytoplasmic tail, but as previously demonstrated the change likely occurs at the pore (Khakh et al., 1999; Virginio et al., 1999b). Our data favor the model in

which channels go from closed to open 1 ($I_1$; pore diameter 11 Å) and then to open 2 ($I_2$; pore diameter >14 Å) during a conformational change(s) in the C tail domain. This conformational change(s) proceeds at a rate of 0.5 $s^{-1}$.

In the conventional view, the shape change in the permeation pathway during permeability changes is occurring on the axis of the multimeric channel, in a region where the cytoplasmic tails of several subunits approach the axis. Recent biochemical and electrophysiological evidence indicates that the $NH_2$ and COOH termini are close to one another in functional $P2X_2$ channels (Boue-Grabot et al., 2000), suggesting at the very least that the cytoplasmic regions are ordered and structured, and lending credence to the idea that these regions could contribute to the inner aspect of a conduction pathway. Consistent with this hypothesis are recent data on nicotinic channels (Miyazawa et al., 1999), *Shaker* (Sokolova et al., 2001), and $Na^+$ channels (Sato et al., 2001), revealing the existence of cytoplasmic hanging baskets that split the conduction pathway. If such fenestrations also occur for P2X channels, then there might be multiple parallel and radially symmetric dilations of the conduction path.

The COOH-terminal tails of $P2X_2$ channels contain several Pro-rich regions, which often bind other proteins (Fig. 5). Work published since submission of this paper has identified protein partners for the $P2X_7$ channel (Kim et al., 2001), and it is possible that a similar situation exists for $P2X_2$ channels. Thus, permeability changes might involve interactions with other cytoplasmic partners, which may differ between $mP2X_2$ and $rP2X_2$ at the crucial two residues we have identified in this study. In particular, it has not escaped our attention that phosphorylation events on a time scale of milliseconds to seconds might participate in the transition to the $I_2$ state. Indeed, $P2X_2$ channel kinetics appear to be regulated by phosphorylation (Boue-Grabot et al., 2000). A further possibility is that the C tail domain itself may not line the pore directly, but may be involved in the conformational change that allows the pore to dilate. In this scenario, the residues that lead to absence of $I_2$ would effectively 'lock' the C tail in a nonpermissive state (Fig. 9). In such a model the transition from the $I_1$ to the $I_2$ state might involve extensive changes in the C tail domain. A large shape change was recently suggested for the gating of the MscL channel (Sukharev et al., 2001): the location of the C tail domain would change during opening as it moves radially from the inner aspect of the pore. Because MscL and P2X channels have similar membrane topologies and both permeate large ions (Khakh, 2001), it is possible to consider that a similar gating mechanism may operate. The above hypotheses reveal several avenues of future experiments to better understand the contribution of the C tail domain to permeability changes at $P2X_2$ channels, but solving the channel structure at atomic resolution in the closed and open states, and deciphering the nature of the transitions, may provide the only completely satisfying view.

We thank K. Kostenko and H. Li for help with preparation of *Xenopus* oocytes, G. Shapovalov for measurements of 2-(methylamino)-ethanol mobility, other members of the group for comments, and Nigel Unwin for discussion and comments on the paper.

Work in our labs was supported by a Wellcome Trust (UK) Prize Fellowship, Roche Bioscience, National Institutes of Health (NS-11756), and the Medical Research Council.

*Submitted: 20 November 2001*
*Revised: 13 May 2002*
*Accepted: 15 May 2002*

REFERENCES

Barry, P.H., and J.W. Lynch. 1991. Liquid junction potentials and small cell effects in ptach-clamp analysis. *J. Membrane Biol.* 121: 101–117.

Boue-Grabot, E., V. Archambault, and P. Seguela. 2000. A protein kinase C site highly conserved in P2X subunits controls the desensitization kinetics of P2X(2) ATP-gated channels. *J. Biol. Chem.* 275:10190–10195.

Cohen, B.N., C. Labarca, N. Davidson, and H.A. Lester. 1992. Mutations in M2 alter the selectivity of the mouse nicotinic acetylcholine receptor for organic and alkali metal cations. *J. Gen. Physiol.* 100:373–400.

Ding, S., and F. Sachs. 1999a. Single channel properties of $P2X_2$ purinoceptors. *J. Gen. Physiol.* 113:695–720.

Ding, S., and F. Sachs. 1999b. Ion permeation and block of $P2X_2$ purinoceptors: single channel recordings. *J. Membr. Biol.* 172: 215–223.

Ding, S., and F. Sachs. 2000. Inactivation of $P2X_2$ purinoceptors by divalent cations. *J. Physiol.* 522:199–214.

Dwyer, T.M., D.J. Adams, and B. Hille. 1980. The permeability of the endplate channel to organic cations in frog muscle. *J. Gen. Physiol.* 75:469–492.

Egan, T.M., W.R. Haines, and M.M. Voigt. 1998. A domain contributing to the ion channel of ATP-gated $P2X_2$ receptors identified by the substituted cysteine accessibility method. *J. Neurosci.* 18: 2350–2359.

Ennion, S., S. Hagan, and R.J. Evans. 2000. The role of positively charged amino acids in ATP recognition by human $P2X_1$ receptors. *J. Biol. Chem.* 275:29361–29367.

Evans, R.J., C. Lewis, C. Virginio, K. Lundstrom, G. Buell, A. Surprenant, and R.A. North. 1996. Ionic permeability of, and divalent cation effects on, two ATP-gated cation channels (P2X receptors) expressed in mammalian cells. *J. Physiol.* 497:413–422.

Gu, B.J., W. Zhang, R.A. Worthington, R. Sluyter, P. Dao-Ung, S. Petrou, J.A. Barden, and J. Wiley. 2001. A Glu-496 to Ala polymorphism leads to loss of function of the human $P2X_7$ receptor. *J. Biol. Chem.* 276:11135–11142.

Haines, W.R., K. Migita, J.A. Cox, T.M. Egan, and M.M. Voigt. 2001. The first transmembrane domain of the P2X receptor subunit participates in the agonist-induced gating of the channel. *J. Biol. Chem.* 276:32793–32798.

Hille, B. 1992. Ionic channels of excitable membranes. 2nd Edition.

Jiang, L.H., F. Rassendren, V. Spelta, A. Surprenant, and R.A. North. 2001. Amino acid residues involved in gating identified in the first membrane-spanning domain of the rat P2X(2) receptor.

*J. Biol. Chem.* 276:14902–14908.

Jiang, L.-H., F. Rassendren, A. Surprenant, and R.A. North. 2000. Identification of amino acid residues contributing to the ATP binding site of a P2X receptor. *J. Biol. Chem.* 275:34190–34196.

Khakh, B.S., P.P. Humphrey, and A. Surprenant. 1995. Electrophysiological properties of P2X-purinoceptors in rat superior cervical, nodose and guinea-pig coeliac neurones. *J. Physiol.* 484:385–395.

Khakh, B.S., X. Bao, C. Labarca, and H.A. Lester. 1999. Neuronal P2X receptor-transmitter-gated cation channels change their ion selectivity in seconds. *Nat. Neurosci.* 2:322–330.

Khakh, B.S., and H.A. Lester. 1999. Dynamic selectivity filters in ion channels. *Neuron.* 23:653–658.

Khakh, B.S. 2001. Molecular physiology of P2X receptors and ATP signalling at synapses. *Nat. Rev Neurosci.* 2:165–174.

Kielland, J. 1937. Individual activity coefficients of ions in aqueous solutions. *J. Am. Chem. Soc.* 59:1675–1678.

Kim, M., L.H. Jiang, H.L. Wilson, R.A. North, and A. Surprenant. 2001. Proteomic and functional evidence for a P2X7 receptor signalling complex. *EMBO J.* 20:6347–6358.

Koshimizu, T., M. Koshimizu, and S.S. Stojilkovic. 1999. Contributions of the C-terminal domain to the control of P2X receptor desensitization. *J. Biol. Chem.* 274:37651–37657.

Koshimizu, T.-A., M. Tomi, M. Koshimizu, and S.S. Stojilkovic. 1998. Identification of amino acid residues contributing to desensitization of the $P2X_2$ receptor channel. *J. Biol. Chem.* 273: 12853–12857.

Migita, K., W.R. Haines, M.M. Voigt, and T.M. Egan. 2001. Polar residues of the second transmembrane domain influence cation permeability of the ATP-gated $P2X_2$ receptor. *J. Biol. Chem.* 276: 30934–30941.

Miyazawa, A., Y. Fujiyoshi, M. Stowell, and N. Unwin. 1999. Nicotinic acetylcholine receptor at 4.6 A resolution: transverse tunnels in the channel wall. *J. Mol. Biol.* 288:765–786.

Ng, B., and P.H. Barry. 1995. The measurment of ionic conductivities and mobilities of certain less common organic ions needed for junction potential corrections in electrophysiology. *J. Neurosci. Methods.* 56:37–41.

North, R.A. 1996. Families of ion channels with two hydrophobic segments. *Curr. Opin. Cell Biol.* 8:474–483.

Rassendren, F., G. Buell, A. Newbolt, R.A. North, and A. Surprenant. 1997. Identification of amino acid residues contributing to the pore of a P2X receptor. *EMBO J.* 16:3446–3454.

Sato, C., Y. Ueno, K. Asai, K. Takahashi, M. Sato, A. Engel, and Y. Fujiyoshi. 2001. The voltage-sensitive sodium channel is a bell-shaped molecule with several cavities. *Nature.* 409:1047–1051.

Simon, J., E.J. Kidd, F.M. Smit, I.P. Chessell, R. Murrell-Lagnado, P.P. Humphrey, and E.A. Barnard. 1997. Localization and functional expression of splice variants of the P2X2 receptor. *Mol. Pharmacol.* 52:237–248.

Smith, F.M., P.P.A. Humphrey, and R.D. Murrell-Lagnado. 1999. Identification of amino acids within the $P2X_2$ receptor C-terminus that regulate desensitization. *J. Physiol.* 520:91–99.

Sokolova, O., L. Kolmakova-Partensky, and N. Grigorieff. 2001. Three-dimensional structure of a voltage-gated potassium channel at 2.5 nm resolution. *Structure.* 9:215–220.

Stoop, R., S. Thomas, F. Rassendren, E. Kawashima, G. Buell, A. Surprenant, and R. North. 1999. Contribution of individual subunits to the multimeric $P2X_2$ receptor: estimates based on methanethiosulfonate block at T336C. *Mol. Pharmacol.* 56:973–981.

Sukharev, S., M. Betanzos, C.S. Chiang, and H.R. Guy. 2001. The gating mechanism of the large mechanosensitive channel MscL. *Nature.* 409:720–724.

Surprenant, A., F. Rassendren, E. Kawashima, R.A. North, and G. Buell. 1996. The cytolytic P2Z receptor for extracellular ATP identified as a P2X receptor ($P2X_7$). *Science.* 272:735–738.

Torres, G.E., T.M. Egan, and M.M. Voigt. 1998. Topological analysis of the ATP-gated ionotropic $P2X_2$ receptor subunit. *FEBS Lett.* 425:19–23.

Unwin, N. 1995. Acetylcholine receptor channel imaged in the open state. *Nature.* 373:37–43.

Virginio, C., A. MacKenzie, R.A. North, and A. Surprenant. 1999a. Kinetics of cell lysis, dye uptake and permeability changes in cells expressing the rat P2X7 receptor. *J. Physiol.* 519:335–346.

Virginio, C., A. MacKenzie, F.A. Rassendren, R.A. North, and A. Surprenant. 1999b. Pore dilation of neuronal P2X receptor channels. *Nat. Neurosci.* 2:315–321.